# Novel Fluorinated Biphenyl Compounds Synthesized via Pd(0)-Catalyzed Reactions: Experimental and Computational Studies

Muhammad Atta Ur Rehman, Muhammad Adeel,* Saad M. Alshehri, Ume Aiman, Alexander Villinger, Saifullah Bullo, Rabia Baby, Muhammad Adnan Asghar, Aleksey E. Kuznetsov,* and Muhammed Lamin Sanyang*

Read Online

ACCESS | Metrics & More | Article Recommendations | SI Supporting Information

**ABSTRACT:** Five new difluorinated biphenyl compounds, 4′-(tert-butyl)-3,4-difluoro-1,1′-biphenyl (**TBDFBP**), 1-(3′,4′-difluoro-[1,1′-biphenyl]-4-yl)ethanone (**DFBPE**), 3′,4′-difluoro-2,5-dimethoxy-1,1′-biphenyl (**DFDMBP**), 3,4-difluoro-3′-nitro-1,1′-biphenyl (**DFNBP**), and (3′,4′-difluoro-[1,1′-biphenyl]-3-yl)-(methyl)sulfane (**DFBPMS**), have been successfully synthesized by the well-known Suzuki−Miyaura coupling with excellent yields averaging 78%. UV−visible, Fourier transform infrared ,and $^{13}$C NMR and $^1$H NMR spectroscopies along with single-crystal X-ray diffraction (SC-XRD) analysis (for **TBDFBP and DFBPE**) were used for the structure elucidation of the synthesized compounds. The SC-XRD results demonstrated the crystal systems of the studied compounds, **TBDFBP** and **DFBPE**, to be monoclinic, and their space groups were found to be $P2_1/c$. Also, a detailed density functional theory study was performed. The calculated structures for **TBDFBP and DFBPE** were found to agree quite well with the experimental results. The natural bonding orbital charge analysis suggested that molecules of these compounds should interact quite noticeably with each other in the solid phase and with polar solvent molecules. Molecular electrostatic potential analysis suggests that accumulation of positive and negative potential implies possibility of quite significant dipole−dipole intermolecular interactions in crystals of these compounds, as well as quite strong interactions with polar solvent molecules. The global reactivity parameters analysis suggests all compounds to be quite stable in redox reactions, with the compound **DFNBP** being relatively more reactive and the compounds **TBDFBP** and **DFDMBP** being relatively more stable.
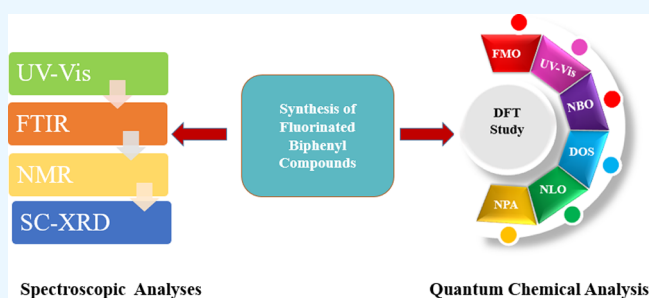
## 1. INTRODUCTION

Aromatic fluorinated biphenyl compounds have progressively achieved considerable significance in several fields of chemistry, such as medicinal chemistry, crop protection, biochemistry, catalysis, and materials science.[1−7] Fluorinated homo- and heteroaromatic compounds are used in medicinal chemistry due to the high electronegativity and small size of fluorine atoms and their high chemical and biological stability. Fluorine changes the electronic distribution and reactivity, which increases drug−receptor interactions and lipophilicity. Fluorinated motifs have a variety of therapeutic effects, including antimycotic, antimalarial, antituberculosis, antiviral, antibiotic, antidiabetic, antidopaminergic, anti-hyperlipidemia, anti-inflammatory, antihistamine, antidepressant, anti-cancer, and anticonvulsant properties.[8−10] In materials science, fluorinated aryls and polyaryls, due to the outstanding stability of the F−C bond, low polarizability, and small size of fluorine, display very weak intermolecular dispersion interactions and are used as liquid crystal displays, organic solar cells, dye-sensitized solar cells, molecular wires in diodes, and in photoluminescence substances.[11−16] The fluorinated biphenyl

and polyphenyl compounds were synthesized by different coupling reactions, among which one can name the Heck reaction, Glaser coupling, Hiyama coupling, and Suzuki reaction. Among these coupling reactions, the Suzuki reaction is the best procedure for C−C bond formation because boronic acid, the main ingredient in the Suzuki reaction, reacts easily and is not dangerous by nature.[17−19]

The Suzuki−Miyaura (SM) reaction is one of the most extensively utilized processes for synthesizing biphenyl derivatives. SM reactions are mostly carried out with the help of catalysts based on simple or more elaborate Pd complexes. Inspired by the fact that fluorinated biphenyl and polyphenyl compounds can be used in all the abovementioned
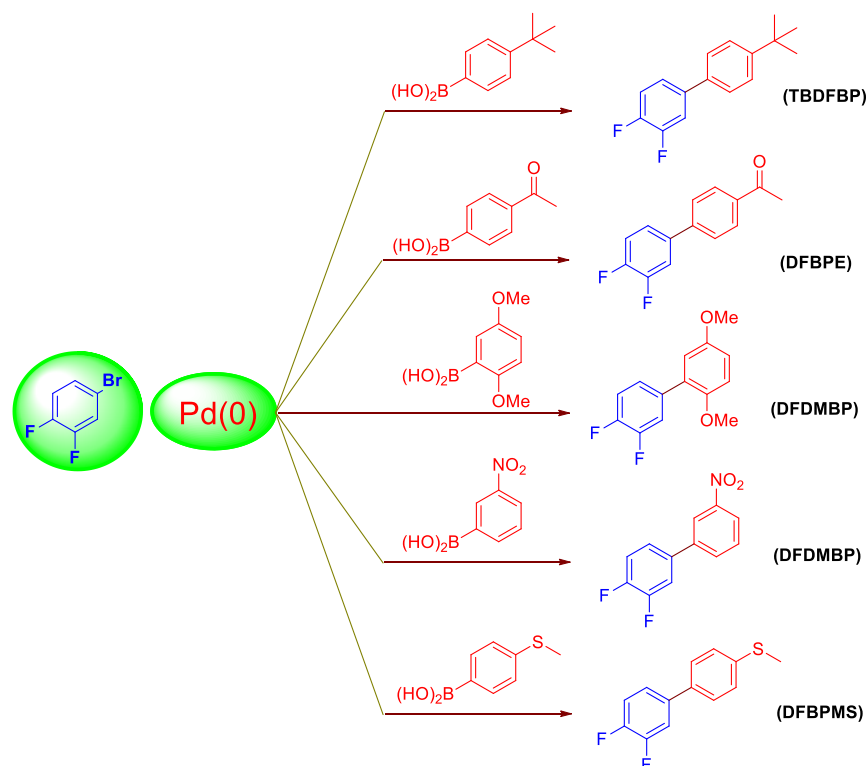
**Scheme 1. General Synthesis of Fluorinated Biaryls**



fields, new fluorinated biphenyls were made using the Suzuki reaction of cross-coupling with Pd catalyst to great effect.

The goal of our research was to use both theoretical and experimental approaches to get insight into the structural and spectroscopic characteristics of the five novel fluorinated biaryl compounds that were synthesized: 4′-(tert-butyl)-3,4-difluoro-1,1′-biphenyl (**TBDFBP**), 1-(3′,4′-difluoro-[1,1′-biphenyl]-4-yl) ethanone (**DFBPE**), 3′,4′-difluoro-2,5-dimethoxy-1,1′-biphenyl (**DFDMBP**), 3,4-difluoro-3′-nitro-1,1′-biphenyl (**DFNBP**), and (3′,4′-difluoro-[1,1′-biphenyl]-3-yl)(methyl) sulfane (**DFBPMS**). Single-crystal X-ray diffraction (SC-XRD) and density functional theory (DFT) studies were employed to receive more information about the structure of the recently obtained fluorinated biaryls. These newly synthesized compounds possess a conjugated π-electronic system along with electrophilic and nucleophilic groups at opposite positions due to which the current flow can take place in such kind of compounds. These compounds are supposed to be used in organic solar cells.

In the next section, materials and methods are described, then results and discussion are given, and finally, conclusions follow.

## 2. EXPERIMENTAL AND COMPUTATIONAL DETAILS

**2.1. General Details.** In this research, analytical-grade chemicals (Merck and Acros) were used. We found the melting points of our compounds with the help of the digital melting point apparatus (A & E Lab, UK). The NMR spectra ($^{13}$C and $^{1}$H) were obtained with the help of the Bruker Avance Neo Technology (75 MHz) and Bruker (300 MHz). Data collection and cell refinement were performed with Bruker Apex V7.51A;[20] data reduction was performed with Bruker *SAINT*; a program used to solve structures was Bruker *SHELXT*;[21] for refining structures, *SHELXL2014/7*[22] was

employed; molecular graphics software used was *ORTEP-3.2.01*.[23]

The IR spectra in the range 400−4000 cm$^{-1}$ were recorded using the Prestige-21 (Shimadzu, Japan) FTIR apparatus. Analytik Jena SPEC ORD 200/210 PLUS was used for the UV−visible spectroscopy.

**2.2. General Techniques for Synthesis of Compounds.** In a pressure tube, starting material 1-bromo-3,4-difluorobenzene (0.1 g, 0.518 mmol), different arylboronic acids (0.777 mmol), $K_3PO_4$ (0.164 g, 0.777 mmol), Pd(PPh$_3$)$_4$ (0.0089 g, 1.5 mol %), and water:dioxane mixture (1:3 v/v ratio) were added and heated at 105 °C for 8.5 h. Thin layer chromatography was used to confirm the target compounds synthesis, and column chromatography was employed to extract the desired pure compounds (silica gel in n-hexane and ethyl acetate solvent system). The obtained compounds were dried before using various spectroscopic techniques to characterize them (See Scheme 1).

*2.2.1. TBDFBP.* The compound **TBDFBP** chemical formula: $C_{16}H_{16}F_2$, melting point was 105−107 °C, percentage yield was 77%, molecular weight 246.30 g/mol. $^{1}$H NMR (300 MHz, CDCl$_3$) δ: 7.6 (s, 4H), 7.5 (s, 2H), 7.4 (m, 1H), 1.35 (s, 9H). $^{13}$C NMR (75 MHz, CDCl$_3$) δ: 151.1 (CF, $J_{CF}$ = 7.5 Hz), 149.1 (CF, $J_{CF}$ = 7.5 Hz), 148.7 (CH), 138.6 (C−C), 136.5 (C−C), 126 (CH), 122.5 (CH), 117.2 (CH, $J_{CF-CH}$ = 12 Hz), 116 (CH, $J_{CF-CH}$ = 13.5 Hz), 115 (CH), 34.5 (t. butyl-H), 31 (CH$_3$). FTIR (cm$^{-1}$): 2961 (s, C−H, Str-sp$^2$), 2840 (m, C−H, Str-sp$^3$), 1603 (m, C−H bending), 1496 (m, C═C). UV−vis ($\lambda_{max}$, ethyl acetate): 256.4 nm (see Supporting Information).

*2.2.2. DFBPE.* The compound **DFBPE** chemical formula: $C_{14}H_{10}F_2O$, the milting point was 71−72 °C, percentage yield 79%, and molecular weight 232.23. $^{1}$H NMR (300 MHz, CDCl$_3$) δ: 8.01 (d, 2H, $J$ = 12 Hz), 7.6 (d, 2H, $J$ = 12.08 Hz), 7.5 (m, 1H), 7.3 (d, 1H, $J$ = 12.7 Hz), 7.2 (d, 1H, $J$ = 12.04
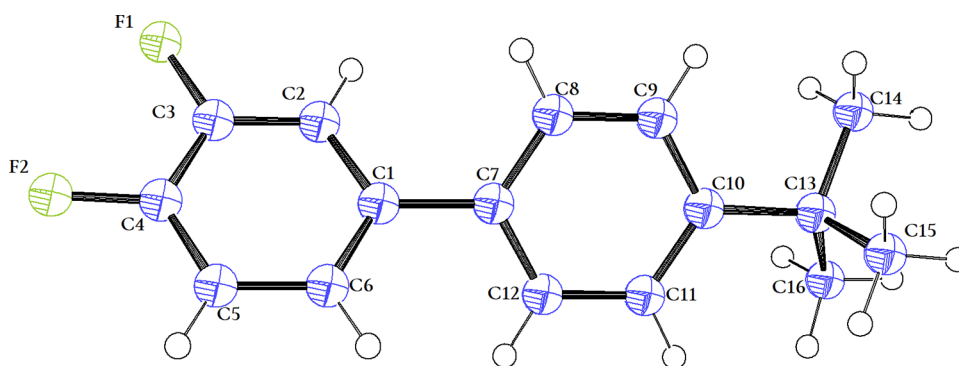
**Figure 1.** ORTEP diagram of the compound **TBDFBP**. Hydrogens are shown by circles of arbitrary radius.

Hz), 2.6 (s, 3H). $^{13}$C NMR (75 MHz, CDCl$_3$) δ: 197.1 (CO), 152.1 (CF, $J_{CF}$ = 7.5 Hz), 149 (CF, $J_{CF}$ = 9.75 Hz), 143.8 (C−C), 136.6 (C−C), 129 (CH), 127.5 (CH), 123.8 (2C), 117 (CH, $J_{CF-CH}$ = 12.75 Hz), 116 (CH, $J_{CF-CH}$ = 12.75 Hz), 26 (CH$_3$). FTIR (cm$^{-1}$): 3061 (m, C−H, aromatic str), (s), 2853 (s, C−H, sp$^3$ str), 1717 (m, C=O, ketones), 1596 (m, C−H bend), 1498 (m, C=C str), 1112 (s, C−O str). UV−vis (λ$_{max}$, ethyl acetate): 275 nm (see Supporting Information).

*2.2.3. DFDMBP.* The compound **DFDMBP** chemical formula: C$_{14}$H$_{12}$F$_2$O$_2$, percentage yield was 72%, and molecular weight 250.24. $^1$H NMR (300 MHz, CDCl$_3$) δ: 7.4 (m, 1H), 7.2 (m, 2H), 6.8 (m, 3H), 3.8 (s, 3H), 3.82 (s, 3H). $^{13}$C NMR (75 MHz, CDCl$_3$) δ: 151 (C−F, $J_{CF}$ = 7.3 Hz), 149 (C−F, $J_{CF}$ = 7.5 Hz), 143.8 (C−C), 136.6 (C−H), 129 (C−H), 127 (C−H), 123.6 (C−H), 118 (CH, $J_{CF}$ = 13.5 Hz), 116 (CH, $J_{CF}$ = 13.5 Hz), 26 (C−CH$_3$). FTIR (cm$^{-1}$): 3000 (m, C−H aromatic str), 2947 (m, C−H sp$^2$ str), 2830 (m, sp$^3$ str), 1604 (m, C−H bending), 1494 (s, C=C str), 1214 (s, C−O str). UV−vis (λ$_{max}$, ethyl acetate): 315.8 nm (see Supporting Information).

*2.2.4. DFNBP.* The **DFNBP** chemical formula: C$_{12}$H$_7$F$_2$NO$_2$, melting point was 92−93 °C, percentage yield 80%, and molecular weight 235.19. $^1$H NMR (300 MHz, CDCl$_3$) δ: 8.4 (s, 1H), 8.2 (d, 1H, $J$ = 12.2 Hz), 7.92 (m, 1H), 7.74 (d, 1H, $J$ = 12.4 Hz), 7.4 (m, 1H), 7.2 (m, 2H). $^{13}$C NMR (75 MHz, CDCl$_3$) δ: 151.1 (CF, $J_{CF}$ = 7.5 Hz), 149.4 (CF, $J_{CF}$ = 7.5 Hz), 148.5 (CNO), 140 (C-C), 135 (CH), 132 (C−H), 130 (C−H), 123 (C−H), 122.8 (C−H), 121 (C−H), 118 (CH, $J_{CF-CH}$ = 12.75 Hz), 116 (CH, $J_{CF-CH}$ = 12.75 Hz). FTIR (cm$^{-1}$): 3084 (m, C−H aromatic str), 2924 (m, C−H sp$^2$ str), 1607 (m, C−H bending), 1511 (s, C=C str), 1350 (s, NO$_2$ sym. str), 1266 (s, N−O str). UV−vis (λ$_{max}$, ethyl acetate): 287.3 nm (see Supporting Information).

*2.2.5. DFBPMS.* The **DFBPMS** melting point was 98−100 °C, yield 80%, chemical formula: C$_{13}$H$_{10}$F$_2$S, and molecular weight 236.2. $^1$H NMR (300 MHz, CDCl$_3$) δ: 7.6 (d, 2H, $J$ = 12.07 Hz), 7.4 (d, 4H, $J$ = 12.03 Hz), 7.2 (s, 1H), 2.5 (s, 3H). $^{13}$C NMR (75 MHz, CDCl$_3$) δ: 152.1 (CF $J_{CF}$ = 7.4 Hz), 148 (CF, $J_{CF}$ = 7.3 Hz), 138 (C−S), 137.6 (C−C), 127.8 (CH), 127.03 (CH), 122 (CH), 117 (CH, $J_{CF-CH}$ = 12.75 Hz), 115 (CH, $J_{CF-CH}$ = 12.75 Hz), 15.8 (S−CH$_3$). FTIR (cm$^{-1}$): 3061 (m, C−H aromatic str), 2921 (m, C−H sp$^2$ str), 1596 (m, C−H bending), 1524 (s, C=C str), 1267 (s, C−S str). UV−vis (λ$_{max}$, ethyl acetate): 262.1 nm (see Supporting Information).

**2.3. Computational Details.** For computational research, the Gaussian 16 program[24] was employed. Starting with the structures obtained from the SC analysis or structures built according to the structural formulas provided, we did geometry optimizations of our compounds using the C1 symmetry (or, in other words, not using any symmetry restrictions at all) followed by calculations of vibrational frequencies and their analysis to make sure that the final structures were indeed energy minima. The hybrid B3LYP[25] functional was combined with the split-valence triple-zeta 6-311+G*[26,27] basis set containing one set of diffuse and one set of polarization functions (the B3LYP/6-311+G* approach). The synthesized compounds were studied computationally both in the vacuum and with the effects of ethyl acetate as an implicit solvent (dielectric constant ε = 5.9867). In the calculations with solvent effects, we employed the self-reliable IEF-PCM technique[28] with the UFF default model used in the Gaussian 16 and with the electrostatic scaling factor α = 1.0. The analysis of atomic charges was done using the natural bond orbital (NBO) method included in the Gaussian 16,[29] with the B3LYP/6-311+G* approach and the implicit solvent effects. Frontier molecular orbitals (FMOs) were computed using the same approach. In the paper, we consider the calculated structures, NBO charges, and FMOs of the five optimized compounds.

Furthermore, the values of the energies of the highest occupied molecular orbitals, HOMOs, and the lowest unoccupied molecular orbitals, LUMOs, were used to define the global reactivity parameters (GRPs) of our compounds[30−32] (eqs 1−6). The values of the ionization potential (IP) and electron affinity (EA) were calculated according to eqs 1 and 2:

$$IP = -E_{HOMO} \tag{1}$$

$$EA = -E_{LUMO} \tag{2}$$

We calculated the global hardness η and electronegativity X values according to eqs 3 and 4:

$$\eta = \frac{[IP - EA]}{2} = -\frac{[E_{LUMO} - E_{HOMO}]}{2} \tag{3}$$

$$X = \frac{[IP - EA]}{2} = -\frac{[E_{LUMO} - E_{HOMO}]}{2} \tag{4}$$

The global electrophilicity ω value was calculated according to eq 5:

$$\omega = \frac{\mu^2}{2\eta} \tag{5}$$

where $\mu = \frac{[E_{HOMO} - E_{LUMO}]}{2}$ is the chemical potential of the system.
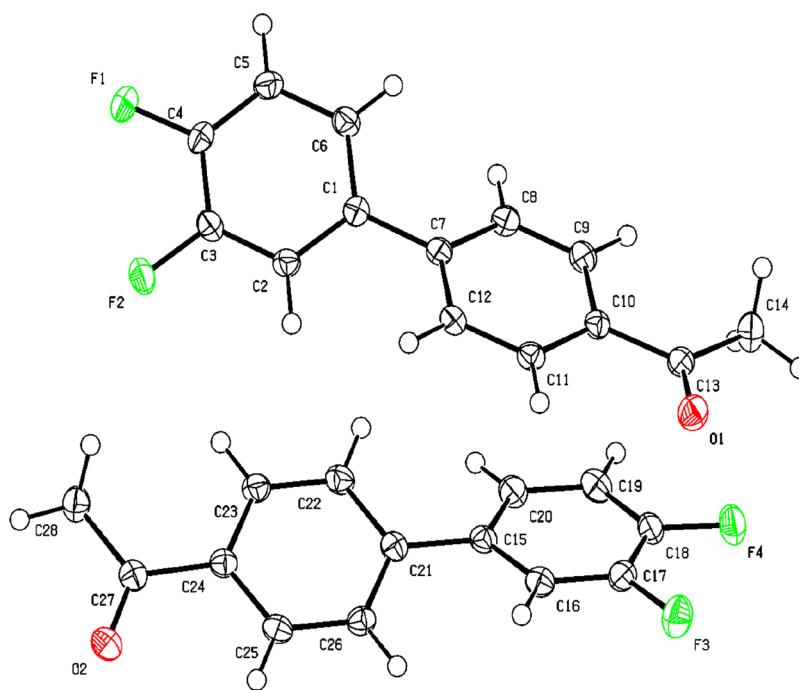
**Figure 2.** ORTEP diagram of the compound **DFBPE**. Hydrogens are shown by circles of arbitrary radius.

The global softness $\sigma$ was calculated according to Eq 6:

$$\sigma = \frac{1}{2\eta} \tag{6}$$

Open GL version of Molden 5.8.2 software was employed to visualize the structures and FMOs of the studied fluorinated biaryls.[33] Avogadro software, version 1.1.1, was used to create images of the molecular electrostatic potential (MEP) maps.[34]

## 3. RESULTS AND DISCUSSION

**3.1. NMR Study Results.** The $^1$H NMR signals confirmed the structure of the **TBDFBP** compound (Figure S11): a singlet peak at 1.386 ppm was attributed to 9 hydrogens of tert-butyl group, another singlet peak at 7.5 was $C_2$ of the fluorinated benzene, and the doublet peak with $J$ = 12.02 (coupling constant) at 7.4 was assigned to 2H of $C_5$ and $C_6$ (cf. Figure 1). A singlet peak at 7.7 was assigned for 4H of C2′, C3′, C5′, and C6′. The $^{13}$C NMR spectrum of the compound **TBDFBP** shows a prominent signal for the methyl and tert-butyl carbons at positions 31 and 34, respectively (Figure S12). The peaks at 116 and 117 are like doublets due to the fluorine-carbon coupling with $J_{CF}$ = 13.5 Hz.

The $^1$H NMR spectrum of the **DFBPE** compound shows six distinct signals (Figure S13). A singlet peak at 2.66 ppm was attributed to three hydrogens in the methyl group. Another singlet peak at 7.29 was $C_2$ of fluorinated benzene (cf. Figure 2). The two doublet peaks with $J$ = 12.03 and 12.1 at 7.7 and 8.1 ppm correspond to 2H of $C_4$, $C_5$ and $C_2$, $C_6$ of the acetylated benzene, respectively. The three singlet peaks at 7.2, 7.3, and 7.4 correspond to H of $C_2$, $C_5$, and $C_6$ of the fluorinated benzene, respectively. The $^{13}$C NMR of the compound **DFBPE** shows a prominent signal for methyl at 26.83 (Figure S14). The peaks at 116 and 117 are like doublets due to the fluorine carbon coupling with $J_{CF}$ = 12.75 Hz. The separate peak at 197.85 indicates the C=O stretching.

The $^1$H NMR spectrum of the **DFDMBP** has five signals (Figure S15). The two singlet peaks at 3.8 and 3.85 ppm reveal

6H from two different methoxy groups. One more singlet peak at 6.8 indicates 3H of the methoxy substituted benzene. The singlet peak at 7.2 ppm was assigned to 2H of the fluorinated benzene. The $^{13}$C NMR of the compound **DFDMBP** shows a prominent signal for the C-F bond at 151 ppm ($j$ (Figure S16)). The peaks at 116 and 117 are like doublets due to the fluorine carbon coupling with $J_{CF}$ = 13.5 Hz. The peak at 26.83 shows the presence of methyl carbon.

Seven distinct signals are seen in the $^1$H NMR spectrum of **DFNBP** (Figure S17). A singlet peak at 7.2 ppm is for 2H of $C_5$ and $C_6$ of the fluorinated benzene. Another singlet peak at 7.3 is $C_2$ of the fluorinated benzene. The four singlet peaks at 7.6, 7.8, 8.1, and 8.3 correspond to 4H of the nitro substituted benzene. The $^{13}$C NMR spectrum of the compound **DFNBP** shows a prominent signal for the C−F group at 151 (Figure S18). The peaks at 116 and 117 are like doublets due to the fluorine carbon coupling with $J_{CF}$ = 12.75 Hz.

For the compound **DFBPMS**, four signals are seen in the $^1$H NMR spectra (Figure S19). A singlet peak at 2.54 ppm is for 3H of the methyl. Another singlet peak at 7.2 is for $C_2$ of the fluorinated benzene. Another two singlet peaks at 7.4 and 7.5 are for 1H of $C_5$ and $C_6$ of the fluorinated benzene. A peak at 7.3 is for 4H of the sulfomethylated benzene. The $^{13}$C NMR spectrum of this compound has a peak at 15.88, which shows the presence of the $CH_3$ group (Figure S20). The prominent signal for C−F is found at 151. The peaks at 116 and 117 are like doublets due to the fluorine carbon coupling with $J_{CF}$ = 12.75 Hz.

**3.2. FTIR Study Results.** The structure of the **TBDFBP** molecule was further validated by the FTIR study (see Figure S1). The FTIR spectrum has peaks at 2951.71 cm$^{-1}$ (approx. 3000 cm$^{-1}$) that indicate the presence of aromatic C−H stretching. By stretching vibrations in the double bond area at 1496 cm$^{-1}$, the aromatic C=C bond was identified. Additionally, the appearance of a peak at 1265.25 cm$^{-1}$ confirmed the $CH_3$ bending vibration.
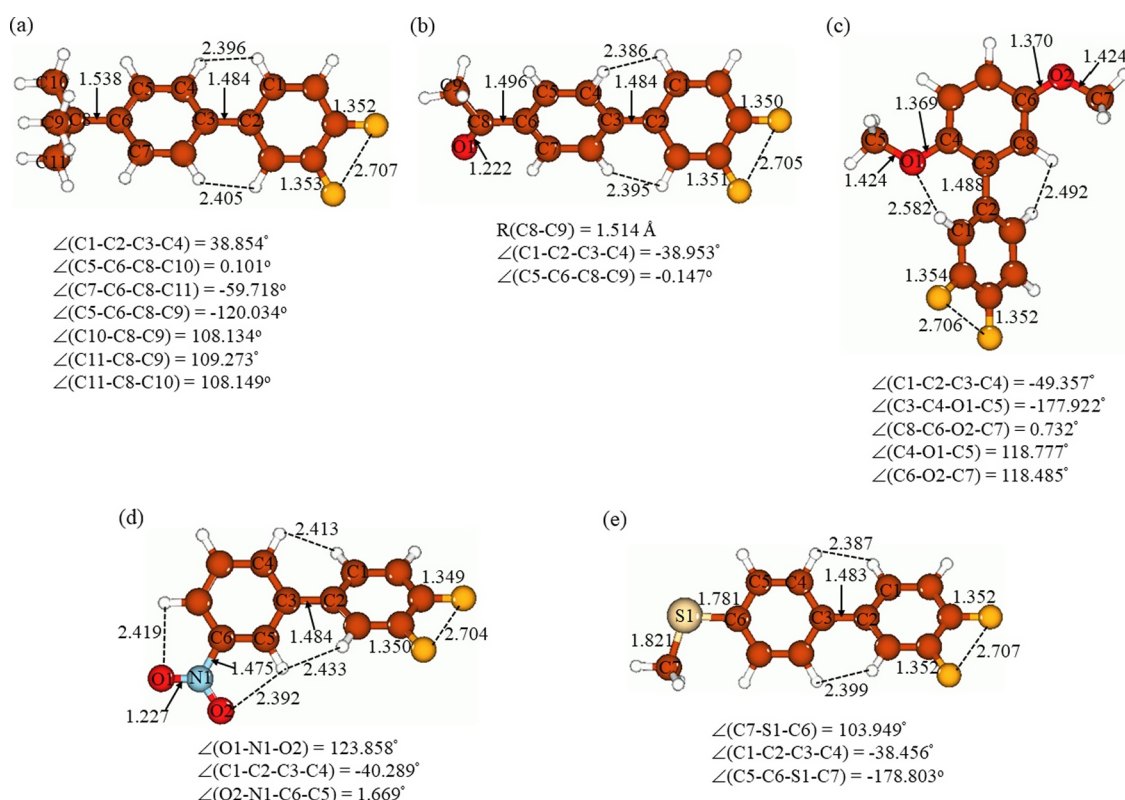
**Figure 3.** Structures of the **TBDFBP** (a), **DFBPE** (b), **DFDMBP** (c), **DFNBP** (d), and **DFBPMS** (e) optimized using the B3LYP/6-311+G* approach with the implicit effects from ethyl acetate. Color coding: brown for C, blue for N, light brown for S, bright yellow for F, red for O, and light gray for H. Bond distances and interatomic distances are in Å, bond angles and dihedral angles are in degrees.

The structure of the molecule **DFBPE** was further confirmed by the FTIR study as well (Figure S2). Its FTIR spectrum has peaks at 2929 and 2857 cm$^{-1}$ indicative of the existence of sp$^2$ and sp$^3$ C—H stretching, respectively. By stretching vibrations in the double bond area at 1496 cm$^{-1}$, the aromatic C=C bond was identified. Additionally, the presence of a peak at 1596 cm$^{-1}$ confirmed the C—H bending vibration. The presence of CO stretching was indicated by a peak at 1717 cm$^{-1}$.

The **DFDMBP** molecule FTIR spectrum has peaks at 2947 and 2830 cm$^{-1}$ that are indicative of the existence of sp$^2$ and sp$^3$ C—H stretching, respectively (Figure S3). By stretching vibrations in the double bond area at 1496 cm$^{-1}$, the aromatic C=C bond was identified. Additionally, the appearance of a peak at 1604 cm$^{-1}$ confirmed the C—H bending vibration. A peak arising at 1214 cm$^{-1}$ confirmed the presence of C—O stretching.

The **DFNBP** molecule FTIR spectrum has a peak at 3084 cm$^{-1}$ that proves the existence of the aromatic C—H stretching (see Figure S4). By stretching vibrations in the double bond area at 1511 cm$^{-1}$, the aromatic C=C bond was identified. Additionally, the presence of a peak at 1607 cm$^{-1}$ confirmed the C—H bending vibration. Furthermore, the C—N$_2$O group was confirmed by a peak at 1350 cm$^{-1}$.

Finally, the **DFBPMS** compound FTIR spectrum has peaks at 2951 and 2913 cm$^{-1}$ that are indicative of the existence of the sp$^2$ and sp$^3$ C—H stretching, respectively (Figure S5). By the presence of the stretching vibration peak in the double bond area at 1496 cm$^{-1}$, the aromatic C=C bond was identified. Additionally, the appearance of a peak at 1607 cm$^{-1}$

confirmed C—H bending vibration. The peak at 1116 cm$^{-1}$ proved the presence of the C—S functionality.

**3.3. UV−Vis Spectroscopy Study.** The UV−vis spectroscopy analysis of the synthesized compounds was done by Analytik Jena SPEC ORD 200/210 PLUS. The compound **TBDFBP** shows maximum absorption of 0.9 A at 256.4 nm (Figure S6), **DFBPE** shows absorption at 0.56 A at 275.7 nm (Figure S7), and **DFDMBP** shows maximum absorption of 0.84 A at 315.8 nm (Figure S8). These results show that these compounds have a continuous pattern of conjugation. **DFNBP** shows maximum absorption of 0.78 A at 287.3 nm (Figure S9), and **DFBPMS** shows maximum absorption of 0.7 A at 262.1 nm (Figure S10).

**3.4. Single-Crystal XRD Data.** *3.4.1. SC-XRD Study of the Compound TBDFBP.* The molecular formula of **TBDFBP** was C$_{16}$H$_{16}$F$_2$. The compound crystal system was found to belong to the monoclinic system, and its space group was defined to be $P2_1/c$. The SC-XRD data were recorded at $T$ = 123 K. All H atoms were positioned geometrically and refined using a riding model, with the following bond lengths, Å: C—H = 0.98 (methyls), 0.99 (methylenes), 1.00 (methines), or 0.95 (aryl CH), and with $U_{iso}(H) = 1.5 \times U_{eq}(C)$ (methyls) or with $U_{iso}(H) = 1.2 \times U_{eq}(C)$ (methylenes, aryl CH, methines). Torsion angles of all methyls were allowed to be refined. The dihedral angle between the newly formed bonds was found to be 39.4°. The ORTEP diagram of **TBDFBP** is given in Figure 1. Further details of the SC-XRD study are provided in Table S1. Table S2 contains selected bond distances and dihedral angles of **TBDFBP**, both experimental and calculated.

*3.4.2. SC-XRD Study of the Compound DFBPE.* The molecular formula of compound **DFBPE** was C$_{14}$H$_{10}$F$_2$O. The
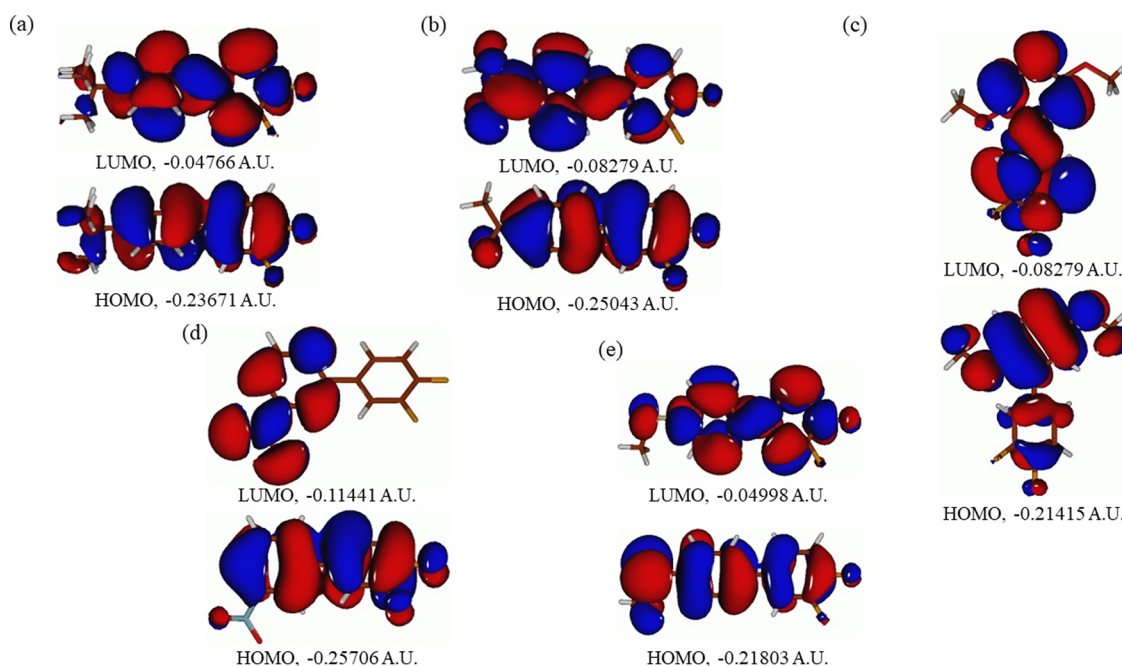
**Figure 4.** Plots of the FMOs for **TBDFBP** (a), **DFBPE** (b), **DFDMBP** (c), **DFNBP** (d), and **DFBPMS** (e) computed with the B3LYP/6-311+G* approach and with the implicit effects from ethyl acetate (isosurface value = 0.015).

compound crystal system was monoclinic, and the space group was determined to be $P2_1/c$. $T$ = 123 K was used to record the data. The dihedral angle between the newly formed bonds was found to be −38.5°. The ORTEP diagram of **DFBPE** is given in Figure 2. Further details of this compound SC-XRD study are provided in Table S1. In Table S2, selected bond distances and dihedral angles of **DFBPE**, both experimental and calculated, are shown.

**3.5. Computational Study.** *3.5.1. Structural Features.* In Figure 3, the singlet structures of the compounds **TBDFBP**, **DFBPE**, **DFDMBP**, **DFNBP**, and **DFBPMS** are provided. Consideration of these structures shows the following. (i) In **TBDFBP**, **DFBPE**, **DFNBP**, and **DFBPMS**, phenyls in the biphenyl moiety are tilted relative to each other by almost the same dihedral angle ($\angle$(C1−C2−C3−C4)), whose absolute values vary within 38.46° (**DFBPMS**−40.29° (**TBDFBP**). However, this dihedral angle becomes noticeably increased, by ca. 9−11°, for **DFDMBP**, which might be ascribed to the more significant steric repulsions between the phenyl ring with two F's and the phenyl ring with two methoxyls, apparently overcoming potential weak hydrogen bonding which might appear between the O of the methoxy group next to the phenyl with two fluorine and the H-atom of that phenyl in ortho-position to the interphenyl bond (O⋯H interatomic distance is 2.582 Å). Also, the C−C bond connecting phenyl in **DFDMBP** is slightly elongated compared to four other compounds, by 0.004−0.005 Å. Also, these more significant steric repulsions between the phenyls in the **DFDMBP** case are supported by somewhat longer O⋯H and H⋯H interatomic distances, 2.582 and 2.492 Å, respectively, compared to slightly shorter H⋯H interatomic distances for other four compounds, 2.386−2.433 Å. Therefore, the phenyl−phenyl orientation is essentially not affected or only slightly affected by varying substituents in one of the phenyl rings. (ii) The C−F bond distances in the compounds considered vary within 1.349−1.354 Å. Also, the interatomic F⋯F distances in all five compounds are very close to each other, varying within 2.704−

2.707 Å. Therefore, the F-containing moieties of the compounds are essentially not affected by the substituents in another phenyl ring. (iii) In the compounds **DFBPE**, **DFDMBP**, **DFNBP**, and **DFBPMS**, the substituting groups prefer to be in the plane of the phenyl rings to which they are attached, which is supported by the following dihedral angles values, degrees: −0.15 ($\angle$(C5−C6−C8−C9), **DFBPE**), −177.92 and 0.73 ($\angle$(C3−C4−O1−C5) and $\angle$(C8−C6−O2−C7), respectively, **DFDMBP**), 1.67 ($\angle$(O2−N1−C6−C5), **DFNBP**), and −178.80 ($\angle$(C5−C6−S1−C7), **DFBPMS**). (iv) In the compounds **DFDMBP** and **DFNBP**, the valence angles for the O-containing groups are slightly different from the ideal value of 120°, being equal to 118.78° and 118.49° for the first compound and 123.86° for the second compound. The valence angle $\angle$(C7−S1−S6) in **DFBPMS** is ca. 104°. (v) Comparison of the DFT structures for the **TBDFBP** and **DFBPE** with their experimental structures (see Table S2), considering such parameters as bond lengths C1−C7 (Figures 1 and 2) and C2 and C3 (Figure 3), C−F bond distances, and torsion angles $\angle$(C2−C1−C7−C12) (Figures 1 and 2) and $\angle$(C1−C2−C3−C4) (Figure 3); O1−C13 (Figure 2) and O1−C8 (Figure 3) show good agreement between the computed and experimental geometries. Some discrepancies could be explained by restricting effects of the crystal structure.

*3.5.2. Frontier MO Analysis.* Figure 4 shows the plots of the HOMOs and LUMOs of the species studied, and Table 1 shows the energies of their FMOs and their HOMO/LUMO and TDDFT gaps, in eV. Analysis of these data shows the following. (i) In the **TBDFBP**, **DFBPE**, **DFNBP**, and **DFBPMS**, the HOMOs are dominated by contributions from essentially the whole molecule; however, in **DFBPMS**, the HOMO has relatively smaller contributions of the fluorines. The contributions from substituents to the HOMOs of **TBDFBP**, **DFBPE**, and **DFNBP** are relatively small, but the **DFBPMS** HOMO is noticeably contributed by the SCH$_3$-group, which can be explained by the diffuse lone pairs with low energies present on the S-atom. (ii) In

**Table 1. FMO Energies of the TBDFBP, DFBPE, DFDMBP, DFNBP, and DFBPMS (eV) along with their HOMO/LUMO and TDDFT Gaps (eV), Calculated at the B3LYP/6-311+G* Level with the Implicit Effects from Ethyl Acetate**

| compound | $E$(HOMO/LUMO), A.U. | $\Delta E$(H/L), eV | $E_{(TDDFT)}$, eV |
|---|---|---|---|
| TBDFBP | −0.23671/−0.04766 | 5.14 | 4.65 |
| DFBPE | −0.25043/−0.08279 | 4.56 | 4.14 |
| DFDMBP | −0.21415/−0.04586 | 4.58 | 3.99 |
| DFNBP | −0.25706/−0.11441 | 3.88 | 3.33 |
| DFBPMS | −0.21803/−0.04998 | 4.57 | 4.12 |

**DFDMBP**, the situation with the HOMO is somewhat different: the contributions from the phenyl with fluorines are relatively small, and the OCH₃-group contributes quite noticeably to the HOMO. (iii) The LUMOs of **TBDFBP**, **DFBPE**, **DFDMBP**, and **DFBPMS** have contributions from the whole molecule, but in the case of **DFNBP**, only the phenyl to which the NO₂-group is bound contributes to the LUMO, along with the NO₂-group itself. (iv) The HOMO/LUMO gap decreases by 0.58 eV from **TBDFBP** (with electron-donating group C(CH₃)₃) to **DFBPE** (with the electron-donating/electron-withdrawing group CH₃−C═O), then very slightly increases, by 0.02 eV, to **DFDMBP** (with electron-donating/electron-withdrawing groups OCH₃), next

further decreases significantly, by 0.70 eV, for **DFNBP** (with strongly electron-withdrawing group NO₂), and finally increases by 0.69 eV for **DFBPMS** (with strongly electron-donating group SCH₃), which has the HOMO/LUMO gap in between the gaps of **DFBPE** and **DFDMBP**. As can be seen from Table 1, the HOMOs are stabilized from **TBDFBP** to **DFBPE**, then destabilized for **DFDMBP**, next again strongly stabilized for **DFNBP**, and strongly destabilized for **DFBPMS**. The LUMOs are strongly stabilized from **TBDFBP** to **DFBPE**, then strongly destabilized for **DFDMBP**, then again very noticeably stabilized for **DFNBP**, and finally strongly destabilized for **DFBPMS**. The TDDFT gaps steadily decrease from **TBDFBP** through **DFNBP** and then again increase for **DFBPMS**, which has the gap very close to the **DFBPE** gap.

These results imply that all five compounds should be quite stable thermodynamically, although the compound **DFNBP** should be relatively less stable.

*3.5.3. Charge Analysis.* In Figure 5, the NBO charges are shown for all the compounds under investigation. Analysis of these charges shows the following. (i) Negative charges on the fluorines and positive charges on the phenyl carbons bound to them vary very slightly with the compound. For the fluorines, the charges vary within −0.343e (**DFNBP**) to −0.349e (**DFDMBP**), and for the carbons, the charges vary within 0.345e−0.356e. Generally, the charge on the carbon in the
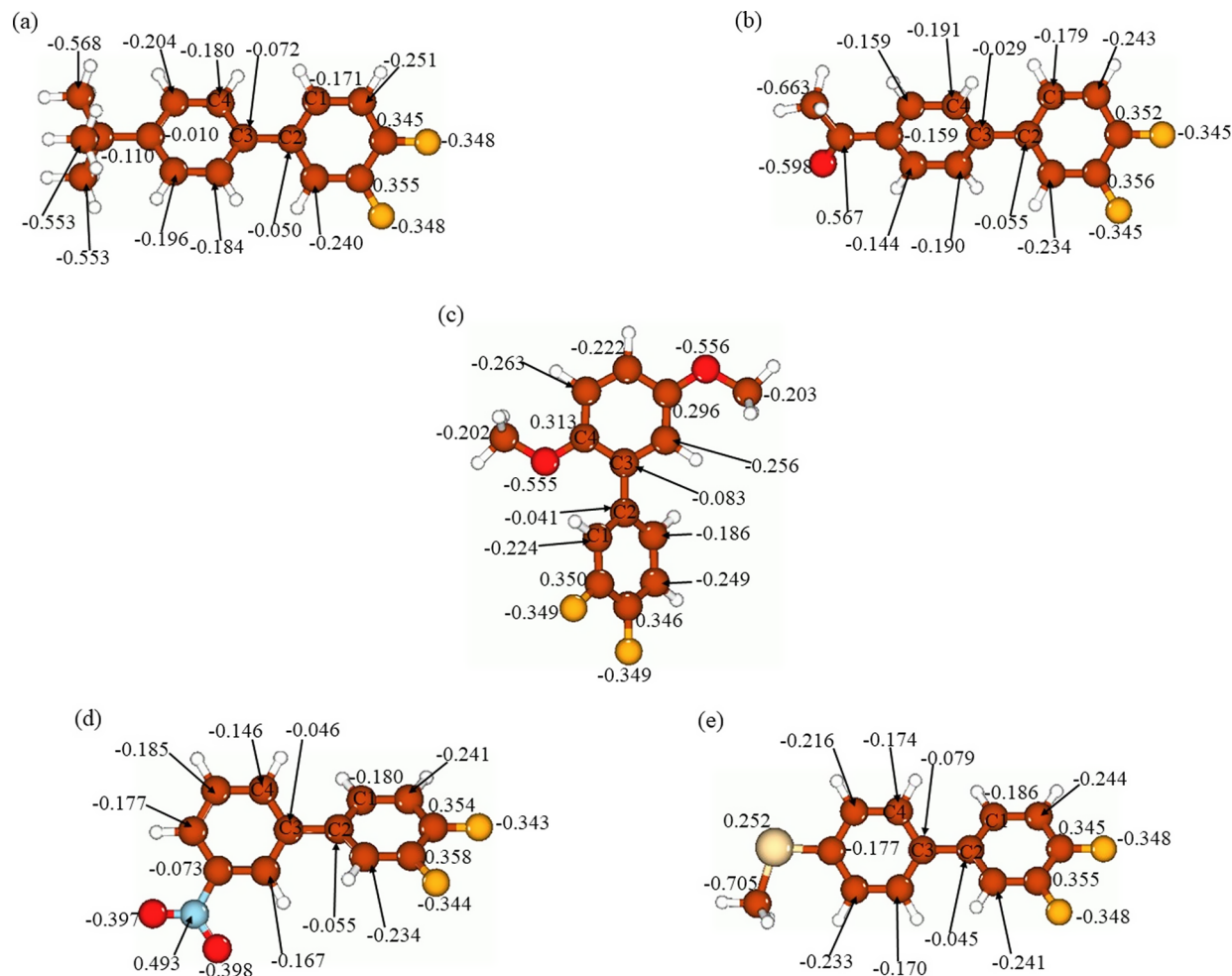


**Figure 5.** NBO charges, e, for the compounds **TBDFBP** (a), **DFBPE** (b), **DFDMBP** (c), **DFNBP** (d), and **DFBPMS** (e) computed at the B3LYP/6-311+G* level with the implicit effects from ethyl acetate.

**Figure 6.** Plots of MEP for **TBDFBP** (a), **DFBPE** (b), **DFDMBP** (c), **DFNBP** (d), and **DFBPMS** (e) computed at the B3LYP/6-311+G* level with the implicit effects from ethyl acetate.
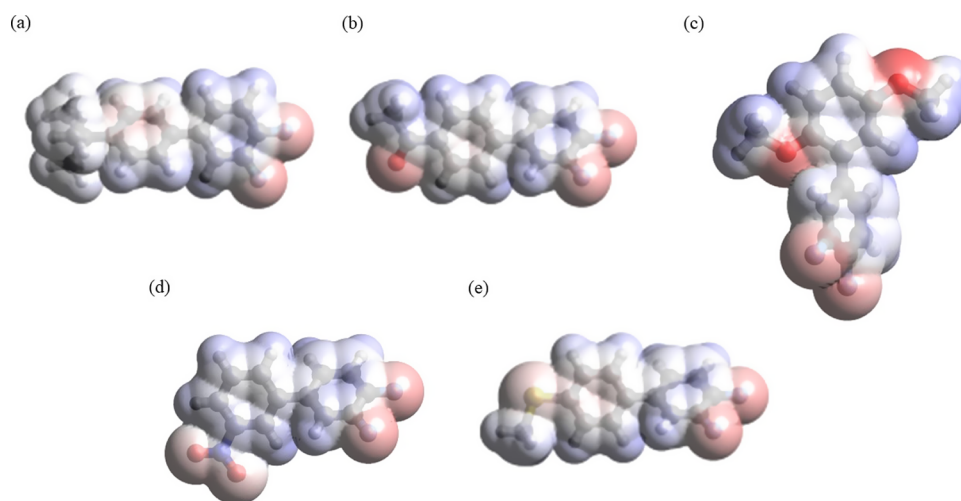
**Table 2. GRPs for the TBDFBP, DFBPE, DFDMBP, DFNBP, and DFBPMS (eV) Calculated at the B3LYP/6−311 + G* Level with the Implicit Effects from Ethyl Acetate**

| compound | $E(H)$ | E(L) | $\Delta E(H/L)$ | IP | EA | $\eta$ | $X$ | $\mu$ | $\omega$ | $\sigma$ |
|---|---|---|---|---|---|---|---|---|---|---|
| **TBDFBP** | −6.44 | −1.30 | 5.14 | 6.44 | 1.30 | 2.570 | 3.870 | −3.870 | 2.914 | 0.195 |
| **DFBPE** | −6.81 | −2.25 | 4.56 | 6.81 | 2.25 | 2.280 | 4.530 | −4.530 | 4.500 | 0.219 |
| **DFDMBP** | −5.83 | −1.25 | 4.58 | 5.83 | 1.25 | 2.290 | 3.540 | −3.540 | 2.736 | 0.218 |
| **DFNBP** | −6.99 | −3.11 | 3.88 | 6.99 | 3.11 | 1.940 | 5.050 | −5.050 | 6.573 | 0.258 |
| **DFBPMS** | −5.93 | −1.36 | 4.57 | 5.93 | 1.36 | 2.285 | 3.645 | −3.645 | 2.907 | 0.219 |

para-position to the C−C interphenyl bond is somewhat smaller, by 0.004−—0.010e, than the charge on the carbon in the meta-position to this bond. (ii) Negative charges on the O-atoms in the compounds **DFBPE**, **DFDMBP**, and **DFNBP** are quite significant, being within −0.397e (**DFNBP**) to −0.598e (**DFBPE**). In the compound **DFNBP**, there is significant positive charge, 0.493e, on the N-atom of the nitro group, and in the compounds **DFBPE** and **DFDMBP**, there are significant positive charges on the carbons of the ethoxy group (**DFBPE**) and phenyl ring (**DFDMBP**) bound to the oxygens, 0.567e and 0.296e−0.313e, respectively. Also, there are noticeable negative charges, ca. −0.2e, on the methoxy carbons in **DFDMBP**. (iii) In **DFBPMS**, there is noticeable positive charge on the S-atom, 0.252e, with significant negative charges on the carbon of the thiomethyl, −0.705e, and on the phenyl carbon, bound to S, −0.177e. Negative charges on the carbons connecting phenyls are relatively low, −0.029e to −0.083e. For the compounds **TBDFBP**, **DFDMBP**, and **DFBPMS**, the charge on the carbon of the phenyl bearing fluorines are smaller than on the carbon of another phenyl, and for two other compounds, the situation is reversed. (v) In the compound **TBDFBP**, the methyl carbons of the tert-butyl group carry significant negative charges, −0.553e to −0.568e. (vi) The carbons of the phenyl rings, which are bound only to hydrogens, carry quite noticeable negative charges in all five compounds, varying within −0.144e and -0.263e.

These results suggest that molecules of the compounds considered should interact quite noticeably with each other in the solid phase, which would assist formation of quite stable crystal phases (see the experimental results above for **TBDFBP** and **DFBPE**). Moreover, the noticeable atomic charges in the molecules of these species would facilitate their dissolution in

polar solvents such as ethyl acetate, water, and dioxane (see above).

*3.5.4. MEP Analysis.* Figure 6 shows the plots of MEP for all five compounds. Analysis of the MEP plots reveals the following aspects. (i) For all five species, there is accumulation of negative MEP (as indicated by red color) on fluorines and accumulations of positive MEP (as indicated by blue color) on the phenyls to which fluorines are connected. Also, the positive potential accumulation can be noticed on hydrogens of the second phenyl and of methyl groups of the substituents. (ii) Slight accumulation of negative MEP can be seen in the second phenyl of **TBDFBP**. (iii) Negative potential accumulations can be seen on oxygens of the O-containing substituents of **DFBPE**, **DFDMBP**, and **DFNBP** as well as on the S-atom of **DFBPMS**. The oxygens in **DFNBP** show somewhat stronger accumulation of negative potential compared to other compounds.

Therefore, the compounds considered might play roles of both electrophiles and nucleophiles in chemical reactions. Moreover, accumulation of positive and negative potential implies the possibility of quite significant dipole−dipole intermolecular interactions in crystals of these compounds, as well as quite strong interactions with polar solvent molecules.

*3.5.5. Global Reactivity Parameters Analysis.* The GRP values were obtained using the FMO energies (Table 1) according to eqs 1−6 (see Computational details) and their computed values in eV are presented in Table 2.

Analysis of the GRPs in Table 2 shows the following. (i) The compound **DFNBP** has the highest IP among the compounds considered, 6.99 eV, followed by **DFBPE**, 6.81 eV, and **TBDFBP**, 6.44 eV, whereas the compound **DFDMBP** has the lowest IP, 5.83 eV. The EA value tendency is similar to the tendency for the IP values: the highest value, 3.11 eV, for

**DFNBP**, then next highest value, 2.25 eV, for **DFBPE**, but the next value, 1.36 eV, is for **DFBPMS**, and again the lowest value, 1.25 eV, is for **DFDMBP**. These results suggest that **DFNBP** would be quite a poor electron donor but quite good electron acceptor, whereas **DFDMBP** would be more prone to lose electrons and less capable to attach them. However, it should be noted that all five compounds have noticeably high values of IP and much lower values of EA, which renders them quite stable in the redox reactions. This is further supported by large HOMO/LUMO gap values, with the highest value, 5.14 eV, for **TBDFBP**. (ii) The compound **TBDFBP** possesses the highest global hardness value in the series, 2.570 eV, whereas the compound **DFNBP** has the lowest global hardness value, 1.940 eV, which implies the lower reactivity and thus increased stability of **TBDFBP** and higher reactivity of **DFNBP**. This is in line with the lowest value of the global softness, 0.195 eV, for **TBDFBP** and the highest value in the series for **DFNBP**, 0.258 eV. These results are also in line with the HOMO/LUMO gap results (see above). It should be noted that three other compounds have essentially the same global softness and global hardness values, thus implying their close relative reactivities. (iii) Global electronegativity and global electrophilicity have highest values in the series for **DFNBP**, 5.050 and 6.573 eV, respectively, whereas **DFDMBP** has the lowest values of these two GRPs, 3.540 and 2.736 eV, respectively. For **TBDFBP,** these parameters have relatively low values as well, 3.870 and 2.914 eV, respectively. These results again support relatively higher reactivity of **DFNBP** and relatively higher stability of **TBDFBP**.

The GRP results imply that all compounds studied should be quite stable in redox reactions. The compound **DFNBP** would be relatively more reactive one, whereas the compounds **TBDFBP** and **DFDMBP** would be relatively more stable.

## 4. CONCLUSIONS

Five new difluorinated diphenyl compounds, namely, **TBDFBP**, **DFBPE**, **DFDMBP**, **DFNBP**, and **DFBPMS**, have been successfully synthesized by the well-known SM coupling with excellent yields averaging 78%, and their structures were confirmed by spectroscopic analysis and single-crystal XRD (for **TBDFBP and DFBPE**). Several features of these compounds such as their structures, FMOs, NBO charges, MEP, and GRPs have also been explored by the DFT study. The calculated structures for **TBDFBP and DFBPE** show good agreement with the experimental geometries. The FMO analysis implies that that all five compounds should be quite stable thermodynamically. The NBO charge analysis suggests that molecules of the compounds considered should interact quite noticeably with each other in the solid phase, which would assist in the formation of quite stable crystal phases. MEP analysis suggests that these compounds might play roles of both electrophiles and nucleophiles in chemical reactions. Moreover, accumulation of positive and negative potential implies the possibility of quite significant dipole—dipole intermolecular interactions in crystals of these compounds, as well as quite strong interactions with polar solvent molecules. The GRP analysis implies that the compounds studied should be quite stable in redox reactions. The compound **DFNBP** would be relatively more reactive one, whereas the compounds **TBDFBP** and **DFDMBP** would be relatively more stable.

## ■ ASSOCIATED CONTENT

**ⓈI Supporting Information**

The Supporting Information is available free of charge at https://pubs.acs.org/doi/10.1021/acsomega.3c01993.

Spectroscopic data (FTIR, SC-XRD, UV−vis, $^{13}$C NMR, and $^{1}$H NMR) (PDF)

## ■ AUTHOR INFORMATION

### Corresponding Authors

**Muhammad Adeel** − *Institute of Chemical Sciences, Gomal University, Dera Ismail Khan 29220 Khyber Pukhtoon Khuwa, Pakistan;* Email: madeel@gu.edu.pk

**Aleksey E. Kuznetsov** − *Departamento de Química, Campus Santiago Vitacura, Universidad Técnica Federico Santa María, Vitacura 7660251, Chile;* ⓞ orcid.org/0000-0001-8857-3118; Email: aleksey.kuznetsov@usm.cl

**Muhammed Lamin Sanyang** − *Directorate of Research and Consultancy, University of The Gambia, Serrekunda 3530, The Gambia;* ⓞ orcid.org/0000-0003-0011-0835; Email: m.sanyang@utg.edu.gm

### Authors

**Muhammad Atta Ur Rehman** − *Institute of Chemical Sciences, Gomal University, Dera Ismail Khan 29220 Khyber Pukhtoon Khuwa, Pakistan*

**Saad M. Alshehri** − *Department of Chemistry, College of Science, King Saud University, Riyadh 11451, Saudi Arabia*

**Ume Aiman** − *Institute of Chemical Sciences, Gomal University, Dera Ismail Khan 29220 Khyber Pukhtoon Khuwa, Pakistan*

**Alexander Villinger** − *Institute of Chemistry, Department of Inorganic Chemistry, University of Rostock, 18059 Rostock, Germany;* ⓞ orcid.org/0000-0002-0868-9987

**Saifullah Bullo** − *Department of Human and Rehabilitation Sciences, Begum Nusrat Bhutto Women University, Sukkur 65200 Sindh, Pakistan*

**Rabia Baby** − *Department of Education, Sukkur IBA University, Sukkur 65200, Pakistan*

**Muhammad Adnan Asghar** − *Department of Chemistry, Division of Science and Technology, University of Education Lahore, Lahore 89002, Pakistan*

Complete contact information is available at:
https://pubs.acs.org/10.1021/acsomega.3c01993

### Notes

The authors declare no competing financial interest.

## ■ ACKNOWLEDGMENTS

## ■ REFERENCES

(1) Jeschke, P. J. C. The unique role of fluorine in the design of active ingredients for modern crop protection. *ChemBioChem* **2004**, *5*, 571−589.

(2) Tian, Y.-M.; Guo, X.-N.; Kuntze-Fechner, M. W.; Krummenacher, I.; Braunschweig, H.; Radius, U.; Steffen, A.; Marder, T. B. Selective photocatalytic C−F borylation of polyfluor-

oarenes by Rh/Ni dual catalysis providing valuable fluorinated arylboronate esters. *J. Am. Chem. Soc.* **2018**, *140*, 17612−17623.

(3) Wang, Y.; Herron, N.; Grushin, V.; LeCloux, D.; Petrov, V. Highly efficient electroluminescent materials based on fluorinated organometallic iridium compounds. *Appl. Phys. Lett.* **2001**, *79*, 449−451.

(4) Bright, T. V.; Dalton, F.; Elder, V. L.; Murphy, C. D.; O'Connor, N. K.; Sandford, G. A convenient chemical-microbial method for developing fluorinated pharmaceuticals. *Org. Biomol. Chem.* **2013**, *11*, 1135−1142.

(5) Wang, B.-C.; Wang, L.-J.; Jiang, B.; Wang, S.-Y.; Wu, N.; Li, X.-Q.; Shi, D.-Y. Application of fluorine in drug design during 2010-2015 years: a mini-review. *Mini Rev. Med. Chem.* **2017**, *17*, 683−692.

(6) Pinto, D. J.; Orwat, M. J.; Wang, S.; Fevig, J. M.; Quan, M. L.; Amparo, E.; Cacciola, J.; Rossi, K. A.; Alexander, R. S.; Smallwood, A. M.; et al. Discovery of 1-[3-(Aminomethyl) phenyl]-N-[3-fluoro-2 '-(methylsulfonyl)-[1, 1 '-biphenyl]-4-yl]-3-(trifluoromethyl)-1 H-pyrazole-5-carboxamide (DPC423), a Highly Potent, Selective, and Orally Bioavailable Inhibitor of Blood Coagulation Factor Xa. *J. Med. Chem.* **2001**, *44*, 566−578.

(7) Menozzi, G.; Merello, L.; Fossa, P.; Schenone, S.; Ranise, A.; Mosti, L.; Bondavalli, F.; Loddo, R.; Murgioni, C.; Mascia, V.; La Colla, P.; Tamburini, E. Synthesis, antimicrobial activity and molecular modeling studies of halogenated 4-[1H-imidazol-1-yl (phenyl) methyl]-1, 5-diphenyl-1H-pyrazoles. *Bioorg. Med. Chem.* **2004**, *12*, 5465−5483.

(8) Thamban Chandrika, N.; Dennis, E. K.; Brubaker, K. R.; Kwiatkowski, S.; Watt, D. S.; Garneau-Tsodikova, S. Broad-Spectrum Antifungal Agents: Fluorinated Aryl-and Heteroaryl-Substituted Hydrazones. *ChemMedChem* **2021**, *16*, 124−133.

(9) Bhagat, S. S.; Rupnar, B. D.; Shirsat, A. J.; Dhas, A. K.; Gill, C. H. Synthesis, Antimicrobial Activity of Substituted Fluoro-N-((1, 3-diphenyl-1H-pyrazol-4-yl) methylene) benzenamines and Fluoro-3-phenyl-2-(1, 3-diphenyl-1H-pyrazol-4-yl) thiazolidin-4-ones. *J. Curr. Pharma Res.* **2019**, *9*, 3275−3282.

(10) Kar, S. S.; Thomas, C. A. Strategically Placed Trifluoromethyl Substituent in the Realm of Antitubercular Drug Design. *Curr. Drug Ther.* **2019**, *14*, 114−123.

(11) Dring, A. M.; Anderson, L. E.; Qamar, S.; Stoner, M. A. Rational quantitative structure−activity relationship (RQSAR) screen for PXR and CAR isoform-specific nuclear receptor ligands. *Chem.-Biol. Interact.* **2010**, *188*, 512−525.

(12) Jiang, Y.; An, Z.; Chen, P.; Chen, X.; Zheng, M. Synthesis and mesomorphic properties of but-3-enyl-based fluorinated biphenyl liquid crystals. *Liq. Cryst.* **2012**, *39*, 457−465.

(13) Hird, M. Fluorinated liquid crystals−properties and applications. *Chem. Soc. Rev.* **2007**, *36*, 2070−2095.

(14) Zhu, M.; Shen, M.; Liang, X.; Chen, H.; Zhu, C.; Du, B.; Luo, D.; Lan, S.; Feng, Z.; Zeng, L. Technology, Identification of Environmental Liquid-Crystal Monomers: A Class of New Persistent Organic Pollutants—Fluorinated Biphenyls and Analogues—Emitted from E-Waste Dismantling. *Environ. Sci. Technol.* **2021**, *55*, 5984−5992.

(15) Zhang, S.; Qin, Y.; Uddin, M. A.; Jang, B.; Zhao, W.; Liu, D.; Woo, H. Y.; Hou, J. A fluorinated polythiophene derivative with stabilized backbone conformation for highly efficient fullerene and non-fullerene polymer solar cells. *Macromolecules* **2016**, *49*, 2993−3000.

(16) de Bettencourt-Dias, A. Lanthanide-based emitting materials in light-emitting diodes. *Dalton Trans.* **2007**, 2229−2241.

(17) Hall, A.; Lacey, D.; Holmes, D. Synthesis and transition temperatures of some branched alkyloxycarbonylphenyl esters of 3-(4'-n-Alkyl-and alkoxy-biphenyl-4-yl) propanoic acids and their laterally fluorinated analogues. *Mol. Cryst. Liq. Cryst. Sci. Technol., Sect. A* **1994**, *250*, 333−346.

(18) Sobhani, S.; Moghadam, H. H.; Skibsted, J.; Sansano, J. M. A hydrophilic heterogeneous cobalt catalyst for fluoride-free Hiyama, Suzuki, Heck and Hirao cross-coupling reactions in water. *Green Chem.* **2020**, *22*, 1353−1365.

(19) Erami, R. S.; Díaz-García, D.; Prashar, S.; Rodríguez-Diéguez, A.; Fajardo, M.; Amirnasr, M.; Gómez-Ruiz, S. Suzuki-Miyaura CC coupling reactions catalyzed by supported Pd nanoparticles for the preparation of fluorinated biphenyl derivatives. *Catalysts* **2017**, *7*, 76.

(20) Madison, W. *APEX2*; Bruker AXS Inc.: USA, 2013.

(21) Sheldrick, G. M. Advances, SHELXT−Integrated space-group and crystal-structure determination. *Acta Crystallogr., Sect. A: Found. Adv.* **2015**, *71*, 3−8.

(22) Sheldrick, G. M. Crystal structure refinement with SHELXL. *Acta Crystallogr., Sect. C: Struct. Chem.* **2015**, *71*, 3−8.

(23) Farrugia, L. J. WinGX and ORTEP for Windows: an update. *J. Appl. Crystallogr.* **2012**, *45*, 849−854.

(24) Frisch, M.; Trucks, G.; Schlegel, H.; Scuseria, G.; Robb, M.; Cheeseman, J.; Scalmani, G.; Barone, V.; Petersson, G.; Nakatsuji, H. *Gaussian 16 Revision C. 01. 2016*; Gaussian Inc., 2016; Vol. *421*.

(25) Beeke, A. D. Density-functional thermochemistry. III. The role of exact exchange. *J. Chem. Phys.* **1993**, *98*, 5648−5652.

(26) McLean, A. D.; Chandler, G. S. Contracted Gaussian basis sets for molecular calculations. I. Second row atoms, Z = 11−18. *J. Chem. Phys.* **1980**, *72*, 5639−5648.

(27) Krishnan, R.; Binkley, J. S.; Seeger, R.; Pople, J. A. Self-consistent molecular orbital methods. XX. A basis set for correlated wave functions. *J. Chem. Phys.* **1980**, *72*, 650−654.

(28) Tomasi, J.; Mennucci, B.; Cammi, R. Quantum mechanical continuum solvation models. *Chem. Rev.* **2005**, *105*, 2999−3094.

(29) Reed, A. E.; Curtiss, L. A.; Weinhold, F. Intermolecular interactions from a natural bond orbital, donor-acceptor viewpoint. *Chem. Rev.* **1988**, *88*, 899−926.

(30) Geerlings, P.; De Proft, F.; Langenaeker, W. Conceptual density functional theory. *Chem. Rev.* **2003**, *103*, 1793−1874.

(31) Chakraborty, A.; Pan, S.; Chattaraj, P. K. Biological activity and toxicity: A conceptual DFT approach. *Applications of density functional theory to biological and bioinorganic chemistry*; 1st ed.; Springer Berlin: Heidellberg, 2013, pp 143−179.

(32) Jorio, S.; Salah, M.; Abou El Makarim, H.; Tabyaoui, M. Reactivity indices related to DFT theory, the electron localization function (ELF) and non-covalent interactions (NCI) calculations in the formation of the non-halogenated pyruvic esters in solution. *Mediterr. J. Chem.* **2019**, *8*, 476−485.

(33) Schaftenaar, G.; Noordik, J. H. J. J. Molden: a pre-and post-processing program for molecular and electronic structures. *J. Comput.-Aided Mol. Des.* **2000**, *14*, 123−134.

(34) Hanwell, M. D.; Curtis, D. E.; Lonie, D. C.; Vandermeersch, T.; Zurek, E.; Hutchison, G. R. Avogadro: An Advanced Semantic Chemical Editor, Visualization, and Analysis Platform. *J. Cheminf.* **2012**, *4*, 1.